Chapter Six

The Orientation Relation between Adjacent Acicular Ferrite Plates and the Measurement of the Dislocation Density for Acicular Ferrite

6.1 Introduction

Acicular ferrite is the most desirable phase in steel weld deposits since its present correlates directly with improved toughness [53-55]. Its transformation mechanism has been known to be displacive where the parent lattice changes into that of the product by some kind of deformation of the former. In these circumstances, the two lattices must always be intimately related [25]. It has been demonstrated [65] that acicular ferrite has a rational (KS/NW type) orientation relation with the austenite. As to the orientation relationship between the adjacent variants of acicular ferrite, some authors [56-58] have proposed a "high-angle" interface between the acicular ferrite plates. Ito et al. [57] stated that the angle was 26° in their research. However, any misorientation between grains should include both an axis and an angle of rotation about that axis to form a complete description [59]. Some authors [56,58] have also suggested that individual acicular ferrite plates contain a relatively high dislocation density, but there are no quantitative data on this. In this Chapter the orientation relation between adjacent variants of acicular ferrite and the dislocation density of acicular ferrite are investigated using transmission electron microscopy. The material studied in this investigation is as-deposited weld metal WD2, and its preparation has been described in Chapter Two. The chemical composition of the weld metal is shown in Table II.1.

6.2 Orientation Relationships between Grains of Identical Structure

The relationship between two cubic crystals X and Y which are of identical structure but which are misorientated with respect to each other can be described in terms of a rotation matrix (Y J X) representing the rigid body rotation which can be imagined to generate crystal Y from crystal X. From the definition of a coordinate transformation matrix [59], each column of (Y J X) gives the components of a basis vector of X in the basis Y. Any rotation of this type, which leaves the common origin of the two crystals fixed, can also be described in terms of a rotation of 180° or less about an axis passing through that origin. If an axis of rotation is represented as a unit vector (or in general, a vector of fixed magnitude), then only three independent quantities are needed to define a misorientation between grains: two components of the axis of rotation, and a right handed angle of rotation. It follows that a rotation matrix must also have only three independent terms. In fact the component of the rotation matrix can be written in term of the vector $\underline{u} = [u_1\ u_2\ u_3]$ which lies along the axis of rotation (such that $u_1u_1 + u_2u_2 + u_3u_3 = 1$),

and in terms of the right-handed angle of rotation θ as follows [59]:

$$(Y\ J\ X) = \begin{pmatrix} u_1u_1(1-m)+m & u_1u_2(1-m)+u_3n & u_1u_3(1-m)-u_2n \\ u_1u_2(1-m)-u_3n & u_2u_2(1-m)+m & u_2u_3(1-m)+u_1n \\ u_1u_3(1-m)+u_2n & u_2u_3(1-m)-u_1n & u_3u_3(1-m)+m \end{pmatrix} \quad \text{(VI.1)}$$

where $m = \cos\theta$ and $n = \sin\theta$

The right-handed angle of rotation can be obtained from the fact that

$$J_{11} + J_{22} + J_{33} = 1 + 2\cos\theta \quad \text{(VI.2)}$$

and the components of the vector $\underline{u}$ along the axis of rotation are given by

$$\begin{aligned} u_1 &= (J_{23} - J_{32}) / (2\sin\theta) \\ u_2 &= (J_{31} - J_{13}) / (2\sin\theta) \\ u_3 &= (J_{12} - J_{21}) / (2\sin\theta) \end{aligned} \quad \text{(VI.3)}$$

It is noted that

$$(Y\ J\ X) = \begin{pmatrix} J_{11} & J_{12} & J_{13} \\ J_{21} & J_{22} & J_{23} \\ J_{31} & J_{32} & J_{33} \end{pmatrix} \quad \text{(VI.4)}$$

There are 24 matrices (as shown in Table VI.1) which represent symmetry rotations in cubic systems, therefore, a cubic bicrystal can be represented in 24 equivalent ways, with 24 axis-angle pairs. Any rotation matrix like (Y J X) when multiplied by rotation matrices representing symmetry operations will lead to the 24 axis-angle pair representations.

6.3 Orientation Relationships between Adjacent Crystallographic Variants of Acicular Ferrite

In addition to intragranular nucleation on inclusions, acicular ferrite also nucleates sympathetically at austenite/acicular ferrite interfaces (Figures II.7c and d), giving rise to an interlocking formation of lenticular plates. Therefore the adjacent variants in intimate contact can arise either from hard impingement between unrelated variants or from sympathetic nucleation. In this section, an attempt is made to find possible orientation relationships between adjacent variants of acicular ferrite. The material used is a high-hardenability weld deposit WD2 as mentioned in Chapter Two. The transmission electron microscopy specimens were prepared from the top layer of as-deposited weld metal.

The results of seventeen experiments are listed in Table VI.2. Eleven examples are illustrated as follows. Figure VI.1 shows the electron micrographs and the corresponding diffraction patterns from a pair of acicular ferrite (α_a) plates A and B. The selected area diffraction patterns (Figures VI.1b,c and d) clearly display that grain A and B have the same zone axis <001>, and a right-handed rotation* of 15° about <001> zone axis would lead to the same orientation between the lattices of grains A and B. This orientation can also be represented by a rotation of 180° about <0.1305 0.9914 0.0000>. Figure VI.2 shows that the acicular ferrite grains B and C also have the same zone axis <001>, and a rotation of 16° about <001> can make the same orientation relation between the lattices of grains B and C. The axis/angle pair relating the grains B and C can also be represented by <0.1392 0.9903 0.0000>/180°. Figure VI.3 shows that the acicular ferrite grains C and D have the same zone axis <001> as well, and a rotation of 13° about <001> will result in the same orientation relation between the lattices of grains C and D. The axis/angle pair relating the grains C and D can also be represented by <0.1132 0.9936 0.0000>/180°. The above results imply that adjacent variants have nearly the same orientation in space, since there is a rotation of ~180° about <001>. This is very significant because even though the variants have nearly the same orientation in space, they have different habit planes (see C-D pair in Figure VI.3). Figure VI.4 shows the electron micrograph and the corresponding diffraction patterns from a pair of acicular ferrite plates E and F. The interface boundary between grains E and F is clearly displayed in Figure VI.4a. The axis/angle pair relating the grains E and F can be demonstrated to be <0.8842 0.2579 0.3894>/174°. Figure VI.5 presents that the acicular ferrite grains G and H have the same zone axis <001> that grains A, B, C and D (Figures VI.1,2 and 3) do, and a rotation of 15° about <001> zone axis would lead to the same orientation between the lattices G and H.

Figure VI.6 shows six acicular ferrite plates designed I, J, K, L, M and N, which are in intimate contact. Figure VI.7 displays the corresponding diffraction patterns from the pair of acicular ferrite plates I and J. It is found that the grains I and J have the same zone axis <1$\bar{1}\bar{1}$>, and a rotation of ~ 0 or 180° will make the same orientation relation between the lattices of grains I and J. These data are ambiguous when the rotation angle about <111> is, within experimental error, ~ 0 or 180°. Because the rotation angle could be 180°, making a twin with this zone axis, it cannot distinguish a twin from two grains which are in identical orientation. Figure VI.8 show that the corresponding diffraction patterns for the pair of acicular ferrite plates I and L have the same zone axis <1$\bar{1}\bar{1}$> as well, and a rotation of 11° about this axis will result in the same orientation. The

* The right-handed sense of rotation about an axis is used in description of axis-angle pairs. Note also that although specific indices are usually quoted for the axes of rotation, the initial choice of basis vectors is of course arbitrary. Therefore the form <001> instead of the form [00$\bar{1}$] is used.

equivalent axis/angle pair for grains I and L can be represented by <0.7430 0.0783 0.6647>/180°. Figure VI.9 shows that the corresponding diffraction patterns for the pair of acicular ferrite plates J and K have the same zone axis <$1\bar{1}\bar{1}$>, and the axis/angle pair <$1\bar{1}\bar{1}$>/11° is the same as that for grains I and L (Figure VI.8). Figure VI.10 shows the corresponding diffraction patterns for the pair of acicular ferrite plates K and L also have the same zone axis <$1\bar{1}\bar{1}$>, and a rotation of ≈ 0 or 180° will make the same orientation for these two grains. As mentioned in Figure VI.7 for the same case, the two grains may be twin-related or in identical orientation. However, the exact orientation relationship cannot be determined without further work. The corresponding diffraction patterns for the pair of acicular ferrite plates L and M are shown in Figure VI.11. These two grains have also the same zone axis <$1\bar{1}\bar{1}$>, and the axis/angle pair can be described by <$1\bar{1}\bar{1}$>/8° or <0.7339 0.0570 0.6769>/180°. Figure VI.12 shows the similar results for the pair of acicular ferrite grains L and M. The axis/angle pair for adjacent grains L and M can be represented by <$1\bar{1}\bar{1}$>/6° or <0.7291 0.0463 0.6828>/180°. From the results shown in Figures VI.6,8,9,11 and 12, the adjacent acicular ferrite pairs I-L, J-K, L-M and L-N seem to be in closer identical orientation, because there is a rotation of ≈180° about <110>. It should be noted again that although the adjacent variants have nearly the same orientation, they have different habit planes.

All the results except the pairs I-J and L-K are listed in Table VI.2, where axis-angle pairs relating adjacent variants of acicular ferrite are presented with the greatest angle of rotation, out of the 24 possibilities for each pair of acicular ferrite plates. Judging from the data, it appears that the adjacent variants have nearly the same orientation in space, since there is a rotation of ≈180° about <001>, or ≈180° about <110>. This is very significant because even though the variants have nearly the same orientation in space, they have different habit planes (for example, C-D, I-L, J-K, L-M and L-N in Figures VI.3 and 6). This is strong evidence for sympathetic nucleation - if the habit planes were not different then the shape change of adjacent variants would be identical and the strain energy would be large and the plates would be parallel. The classical bainitic transformation involves a sympathetic nucleation to form as sheaves, which contain very closer identical orientation related sub-unit ferrite platelets. The fact that the habit plates of adjacent variants of acicular ferrite in approximately the same orientation are not parallel means that the formation of a plate triggers the formation of another whose orientation is nearly the same, but habit plane (and therefore displacement vector) is different, probably in a way which does not oppose the shape change of the original plate. This is like the autocatalytic nucleation found in the classical bursts of martensitic transformation.

6.4 Measurement of the Dislocation Density of Acicular Ferrite

The dislocation structure observed in transmission electron microscopy thin foils can be considered to be equivalent to those existing in bulk material if precautions are taken during the preparation of foils. A minor amount of dislocations may be introduced by mechanical deformation during thinning. It is unlikely that the conventional electrolytic polishing introduces any dislocation into a foil but the subsequent handling of the specimen frequently leads to accidental deformation. The dislocations introduced in this way tend to be long and nearly straight [170] since they lie parallel to the foil surface. This damage is easily recognised with experience and can be avoided in ordinary polycrystalline specimens. Other factors such as surface image forces may make the dislocation leave the foil, but the use of oxidising polishing solutions usually leaves a thin oxide film of the surface of the foil and prevents any such losses. Obviously, the best test for any dislocation distribution which is suspect is the reproducibility from one specimen to another or from one area of a foil to another.

The specimens studied in this investigation were taken from the top layer (fusion zone) of weld metal WD2. The same preparation of thin foils has been described as in Chapter Two. The microscopy was conducted on a Philips EM400T transmission electron microscope operated at 120kV. The dislocation density of acicular ferrite was determined from ten micrographs at the magnifications of 60,000 ~ 100,000X. These magnifications were chosen because they were high enough to resolve individual dislocations and the dislocation density in a micrograph could still be representative of the average dislocation density. Typical micrographs used for determining the dislocation density are shown in Figure VI.13. Ham [171] and Hirsch et al. [170a] showed that provided the dislocations are randomly oriented, their density measured in units of m/m^3 is given by $\rho = 2NM/Lt$, where N is the number of intersections that a random straight test line laid on a transmission electron micrograph makes with the dislocations, L is the total length of the test line, t is the thickness of foil and M is the magnification of the micrograph. In order to minimise any dislocation orientation effects, the method to count the intersections with a series of circles instead of using random straight lines has been used [172,173]. In the present work two concentric circles 4.40 and 6.28cm in circumference were used. The dislocation density of acicular ferrite in different areas of a foil or in different foils has been calculated.

To determine the dislocation density ρ from the relation $\rho = 2NM/Lt$ the foil thickness (t) has to be determined. The foil thickness was calculated by counting extinction contours [170b]: provided the diffraction conditions are such that one reflection is operating (two-beam case) the foil thickness is given by $t = \eta_g \zeta_g$, where η_g is the

number of extinction fringes of acicular ferrite grain for diffraction vector $\vec{g}$ and ζ_g is the extinction distance for the corresponding $\vec{g}$ and electron energy. The thickness is given by $t = \eta_g \zeta_g$ only when the foil is tilted so that the grain examined is at the exact Bragg condition [170b,174] in which the spacing between fringes is a maximum. The main operating reflection was determined by selected area diffraction. If as a result of selected area diffraction it was seen that there was more than one operating reflection, the foil was tilted to the two-beam case. The values of extinction distances (ζ_g) for 120 kV electron energy are given in Table VI.3, which are obtained [170c] from those for 100 kV electron energy by multiplying by a factor $\upsilon 120/\upsilon 100$, where $\upsilon 120$ and $\upsilon 100$ are the velocity of electron at 120 and 100 kV, respectively. A series of micrographs have been taken in bright field with a single strong reflection $\vec{g}$ = 100, 200 or 112. In this study the diffraction conditions of two-beam render some dislocations invisible, however, the percentage of invisible dislocation can easily be calculated if the assumptions are as follows:

(i) All dislocations have Burgers vectors of the type $\vec{b}$ = a/2 <111>, where a is the lattice parameter of acicular ferrite, i.e., all the dislocations are undissociated.

(ii) The dislocations were randomly distributed both in space and among the four possible variants of the Burgers vectors.

(iii) All dislocations satisfying the invisibility criterion ($\vec{g} \cdot \vec{b}$ = o) are completely out of contrast.*

The value of $\vec{g} \cdot \vec{b}$ for the first three reflections and the a/2<111> Burgers vectors in BCC metals are listed in Table VI.5. The proportion of the a/2<111> Burgers vectors invisible in BCC metals under different two-beam diffraction conditions are summarised in Table VI.4.

Electron micrograph Figure VI.13 shows the bright field image of acicular ferrite under the two-beam condition $\vec{g}$ = <1$\bar{2}$1>. It clearly displays 5 extinction fringes on the grain boundary, therefore the thickness of this grain is 2690Å. The average foil thickness for the measurements is of the order of 2455±440Å. After the dislocation density had been measured directly from the electron micrograph, the corrected dislocation density was calculated by adding the part invisible under corresponding two-beam diffraction condition to the measured dislocation density. A complete list of experimental data in this

* In fact, the invisibility criterion $\vec{g} \cdot \vec{b}$ = o can only be applied for screw dislocation. For edge dislocation both $\vec{g} \cdot \vec{b}_e$ and $\vec{g} \cdot \vec{b}_e \wedge \vec{u}$ (where $\vec{b}_e$ and $\vec{u}$ are Burgers vector of edge dislocation and a unit vector along the edge dislocation line, respectively) must all be zero for complete invisibility, which is a very restricted criterion compared with the $\vec{g} \cdot \vec{b}$ = o criterion. However, in practice only faint residual contrast generally occurs for edge dislocation when $\vec{g} \cdot \vec{b}$ = o (i.e., $\vec{g} \cdot \vec{b}_e$ = o), but $\vec{g} \cdot \vec{b}_e \wedge \vec{u} \neq$ o and this has been interpreted as indicating dislocation invisibility [175].

work is presented in Table VI.6. The average corrected dislocation density of acicular ferrite is of the order of (3.90±1.97) x $10^{14}m^{-2}$.

6.5 Summary and Conclusions

The orientation relationship between adjacent acicular ferrite plates has been been studied. It has found that many adjacent variants of acicular ferrite have a very close identical orientation even though they have different habit planes. This is strong evidence for sympathetic nucleation - if the habit planes were not different then the shape change of adjacent variants would be identical and the plates would be parallel, as the case of classical bainite. The fact that the habit planes of variants in nearly the same orientation are not parallel implies that the formation of a plate triggers the formation of another whose orientation is nearly the same, but habit plane (and therefore displacement vector) is different, probably in a way which does not oppose the shape change of the original plate.

The dislocation density of acicular ferrite has also been measured using two-beam technique, and is of the order of $10^{14}m^{-2}$. The high dislocation density is consistent with the high temperature displacive transformation mechanism in which there is some plastic accommodation of the shape change due to transformation.

Table VI.1 - 24 matrices representing all the symmetry rotations in cube systems.

$$\begin{pmatrix}1&0&0\\0&1&0\\0&0&1\end{pmatrix},\quad \begin{pmatrix}\bar{1}&0&0\\0&1&0\\0&0&1\end{pmatrix},\quad \begin{pmatrix}1&0&0\\0&\bar{1}&0\\0&0&1\end{pmatrix},\quad \begin{pmatrix}1&0&0\\0&1&0\\0&0&\bar{1}\end{pmatrix},$$

$$\begin{pmatrix}1&0&0\\0&0&1\\0&1&0\end{pmatrix},\quad \begin{pmatrix}\bar{1}&0&0\\0&0&1\\0&1&0\end{pmatrix},\quad \begin{pmatrix}1&0&0\\0&0&1\\0&\bar{1}&0\end{pmatrix},\quad \begin{pmatrix}1&0&0\\0&0&\bar{1}\\0&1&0\end{pmatrix},$$

$$\begin{pmatrix}0&1&0\\1&0&0\\0&0&1\end{pmatrix},\quad \begin{pmatrix}0&1&0\\\bar{1}&0&0\\0&0&1\end{pmatrix},\quad \begin{pmatrix}0&\bar{1}&0\\1&0&0\\0&0&1\end{pmatrix},\quad \begin{pmatrix}0&1&0\\1&0&0\\0&0&\bar{1}\end{pmatrix},$$

$$\begin{pmatrix}0&0&1\\1&0&0\\0&1&0\end{pmatrix},\quad \begin{pmatrix}0&0&1\\\bar{1}&0&0\\0&1&0\end{pmatrix},\quad \begin{pmatrix}0&0&1\\1&0&0\\0&\bar{1}&0\end{pmatrix},\quad \begin{pmatrix}0&0&\bar{1}\\1&0&0\\0&1&0\end{pmatrix},$$

$$\begin{pmatrix}0&1&0\\0&0&1\\1&0&0\end{pmatrix},\quad \begin{pmatrix}0&1&0\\0&0&1\\\bar{1}&0&0\end{pmatrix},\quad \begin{pmatrix}0&\bar{1}&0\\0&0&1\\1&0&0\end{pmatrix},\quad \begin{pmatrix}0&1&0\\0&0&\bar{1}\\1&0&0\end{pmatrix},$$

$$\begin{pmatrix}0&0&1\\0&1&0\\1&0&0\end{pmatrix},\quad \begin{pmatrix}0&0&1\\0&1&0\\\bar{1}&0&0\end{pmatrix},\quad \begin{pmatrix}0&0&1\\0&\bar{1}&0\\1&0&0\end{pmatrix},\quad \begin{pmatrix}0&0&\bar{1}\\0&1&0\\1&0&0\end{pmatrix}.$$

Table VI.2 - Experimentally determined axis-angle pairs relating adjacent variants of acicular ferrite.

Adjacent Acicular Ferrite Plates	Varient Set*	Axis-Angle Pair	
A-B	1-18	<0.1305 0.9914 0.0000>	180°
B-C	1-18	<0.1392 0.9903 0.0000>	180°
C-D	1-18	<0.1132 0.9936 0.0000>	180°
E-F	1-17	<0.8845 0.2579 0.3894>	174°
G-H	1-18	<0.1305 0.9914 0.0000>	180°
I-J	Description is given in Section 6.2.2		
I-L	1-14	<0.7430 0.0783 0.6647>	180°
J-K	1-14	<0.7430 0.0783 0.6647>	180°
K-L	Description is given in Section 6.2.2		
L-M	1-14	<0.7339 0.0570 0.6769>	180°
L-N	1-14	<0.7291 0.0463 0.6828>	180°
–	1-2	<0.6388 0.6169 0.4596>	179°
–	1-23	<0.2077 0.6092 0.7853>	175°
–	1-10	<0.3676 0.5926 0.7167>	173°
–	1-4	<0.7661 0.6346 0.1016>	175°
–	1-16	<0.4808 0.7974 0.3646>	179°
–	1-21	<0.4828 0.1684 0.8594>	175°

*One of the 24 equivalent axis-angle pairs, with the greatest angle of rotation is chosen for each pair of adjacent acicular ferrite plates in order to interpret easily.

Table VI.3 - Extinction distance ζ_g (Å) in ferrite for 100 and 120 kV electron energy, respectively.

Reflection $\vec{g}$	Extinction distance ζ_g (Å)	
	100 kV	120 kV
110	270	289
200	395	423
211	503	538
220	606	648
310	712	762

Table VI.4 - Proportion of Burgers vectors a/2 <111> invisible in BBC lattice under different two-beam diffraction conditions.

Diffraction conditions	Proportion of invisible Burgers vectors
Two-beam	
$\vec{g}$ = <110>	0.5
$\vec{g}$ = <200>	0
$\vec{g}$ = <211>	0.25

Table VI.5 - The volume of $\vec{g}\vec{b}$ for the first three reflections and the a/2 <111> Burgers vectors in BCC lattice.

Reflection	Possible Burgers vector (times a/2) 1/2[111]	1/2[$\bar{1}$11]	1/2[1$\bar{1}$1]	1/2[11$\bar{1}$]
110	1	0	0	1
101	1	0	1	0
011	1	1	0	0
$\bar{1}$10	0	1	$\bar{1}$	0
$\bar{1}$01	0	1	0	$\bar{1}$
0$\bar{1}$1	0	0	1	$\bar{1}$
200	1	$\bar{1}$	1	1
020	1	1	$\bar{1}$	1
002	1	1	1	$\bar{1}$
$\bar{2}$00	$\bar{1}$	1	$\bar{1}$	$\bar{1}$
0$\bar{2}$0	$\bar{1}$	$\bar{1}$	1	$\bar{1}$
00$\bar{2}$	$\bar{1}$	$\bar{1}$	$\bar{1}$	1
112	2	1	1	0
121	2	1	0	1
211	2	0	1	1
$\bar{1}$12	1	2	0	$\bar{1}$
$\bar{1}$21	1	2	$\bar{1}$	0
$\bar{2}$11	0	2	$\bar{1}$	$\bar{1}$
1$\bar{2}$2	1	0	2	$\bar{1}$
12$\bar{1}$	0	$\bar{1}$	2	$\bar{1}$
21$\bar{1}$	1	$\bar{1}$	2	0
11$\bar{2}$	0	$\bar{1}$	$\bar{1}$	2
12$\bar{1}$	1	0	$\bar{1}$	2
21$\bar{1}$	1	$\bar{1}$	0	2

Table VI.6 - Experimental data for dislocation density calculation

Two-beam condition $\vec{g}$	No. of extinction fringes η_g	Thickness of thin foil t (Å)	measured dislocation density (m^{-2})	corrected dislocation density (m^{-2})
<112>	5	2690	1.87×10^{14}	2.49×10^{14}
<110>	5	1445	4.90×10^{14}	8.90×10^{14}
<112>	5	2690	2.05×10^{14}	2.73×10^{14}
<200>	6	2538	2.47×10^{14}	2.47×10^{14}
<112>	5	2690	2.60×10^{14}	3.46×10^{14}
<112>	5	2690	2.53×10^{14}	3.37×10^{14}
<110>	6	1734	3.16×10^{14}	6.32×10^{14}
<112>	5	2690	2.18×10^{14}	2.91×10^{14}
<112>	5	2690	2.29×10^{14}	3.05×10^{14}
<112>	5	2690	2.46×10^{14}	3.28×10^{14}

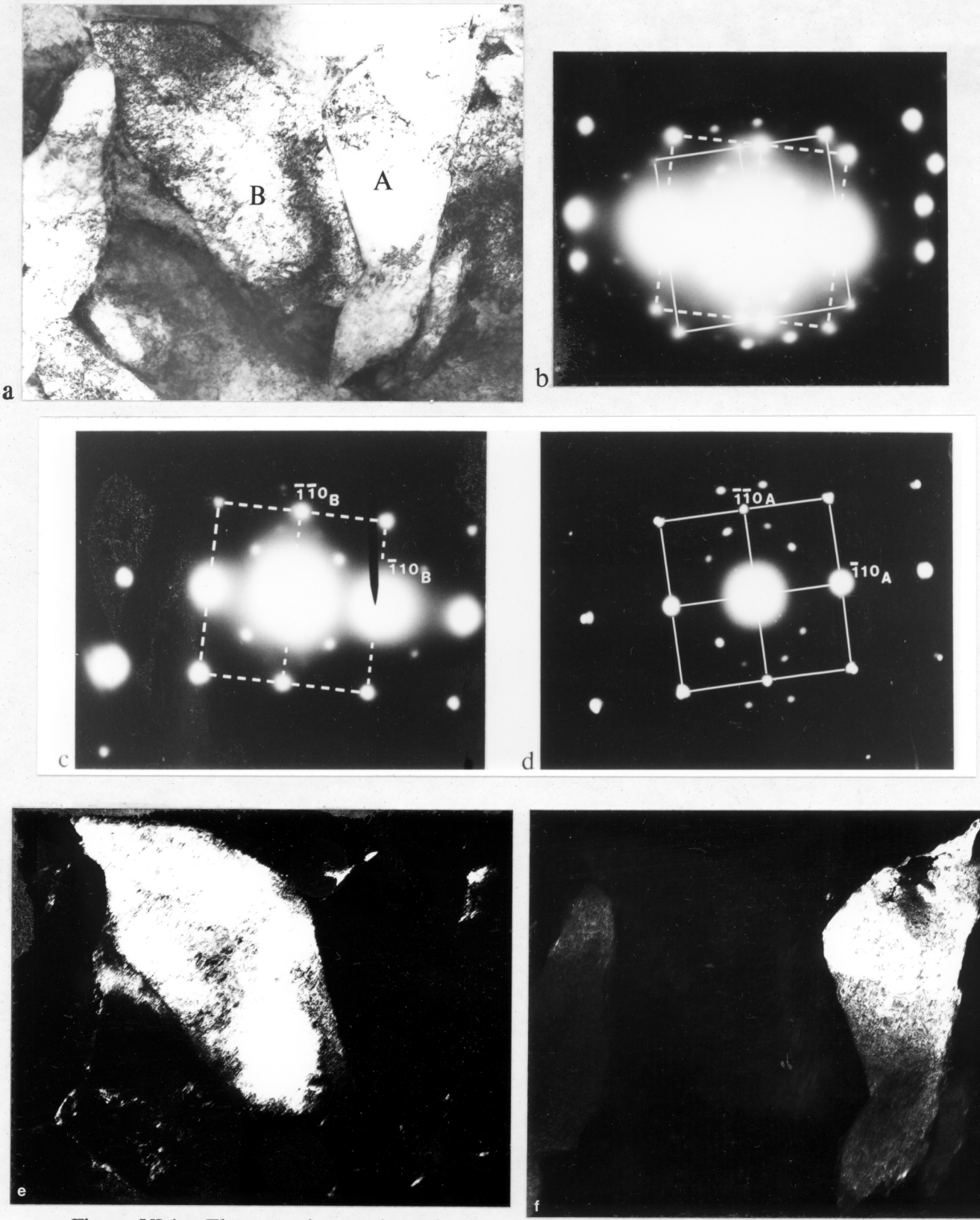

Figure VI.1 - Electron micrographs and corresponding diffraction patterns from a pair of α_a plates A and B. (a) Bright field image. (b) Selected area diffraction pattern (SADP) from interface of grains A and B. (c) SADP from grain B. (d) SADP from grain A. (e) Dark field image of grain B using $(110)_B$ reflection. (f) Dark field image of grain A using $(110)_A$ reflection. The central bright spots are Fe_2O_3 surface oxide reflections.

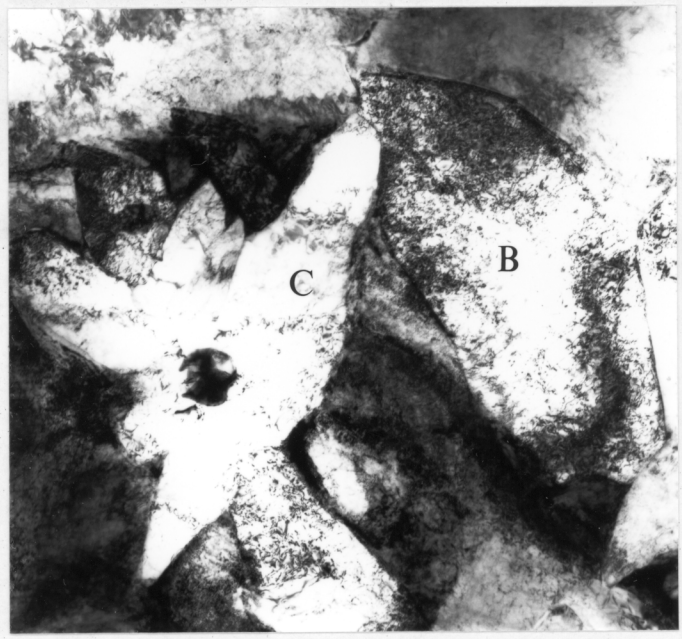

a

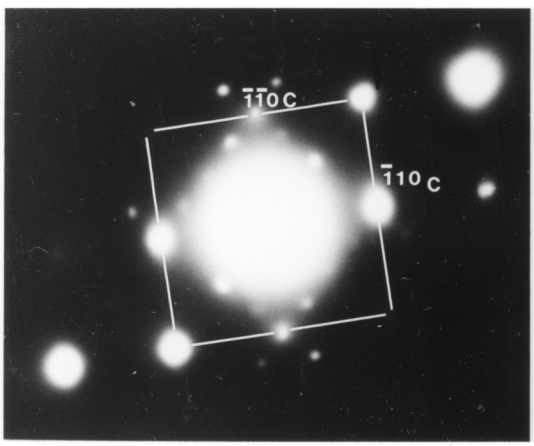

b

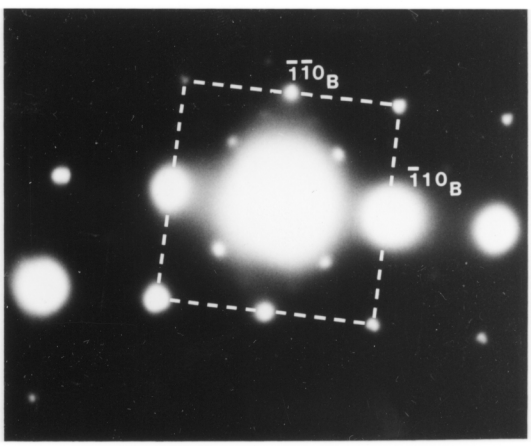

c

d

e

Figure VI.2 - Electron micrographs and corresponding diffraction patterns from a pair of α_a plates B and C. (a) Bright field image. (b) SADP from grain C. (c) SADP from grain B. (d) Dark field image of grain C using $(200)_C$ reflection. (e) Dark field image of grain B using $(110)_B$ reflection. The central bright spots are Fe_2O_3 surface oxide reflections.

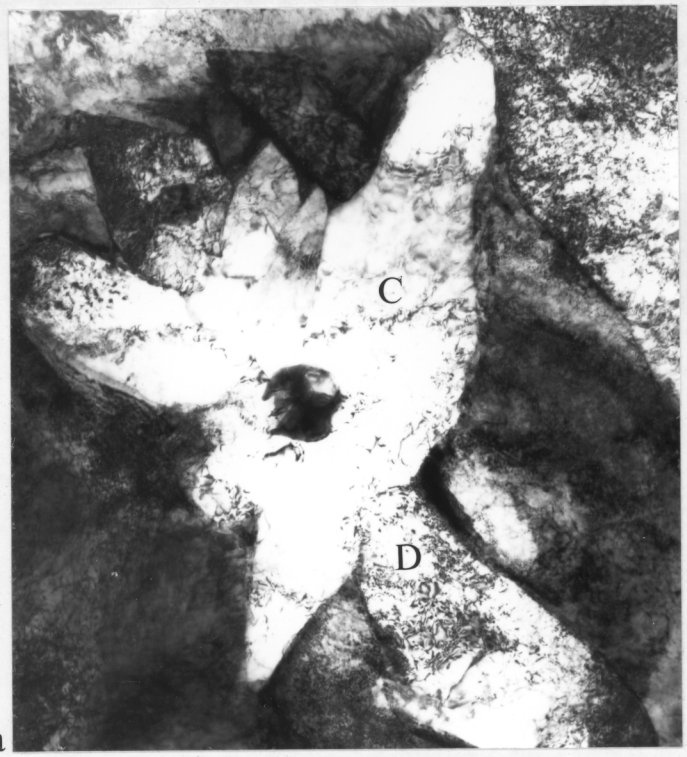

a

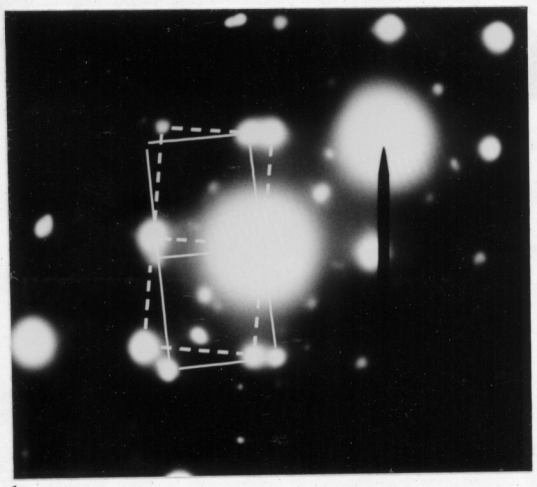

b

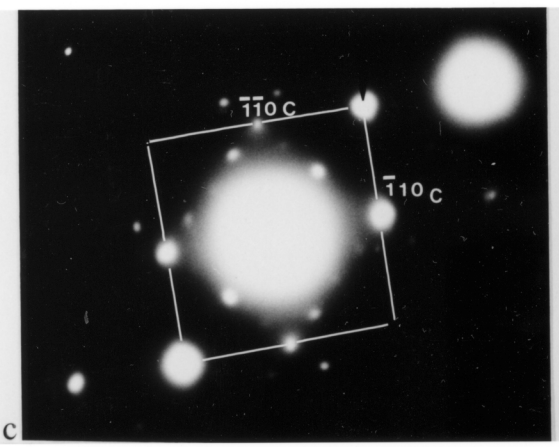

c

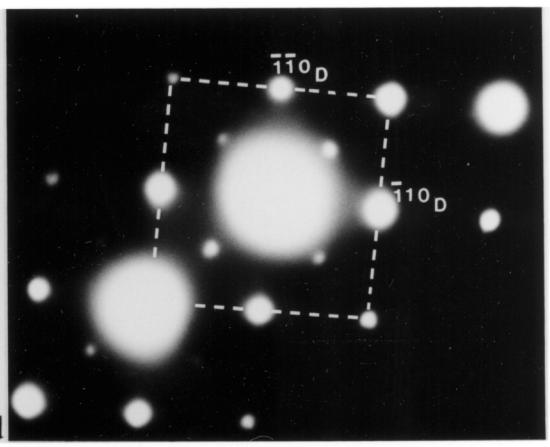

d

e

f

Figure VI.3 - Electron micrographs corresponding diffraction patterns from a pair of α_a plates C and D. (a) Bright field image. (b) SADP from interface of grains C and D. (c) SADP from grain C. (d) SADP from grain D. (e) Dark field image of grain C using $(\bar{2}00)_C$ reflection. (f) Dark field image of grain D using $(200)_D$ reflection. The central bright spots are Fe_2O_3 surface oxide reflections.

1·0 µm

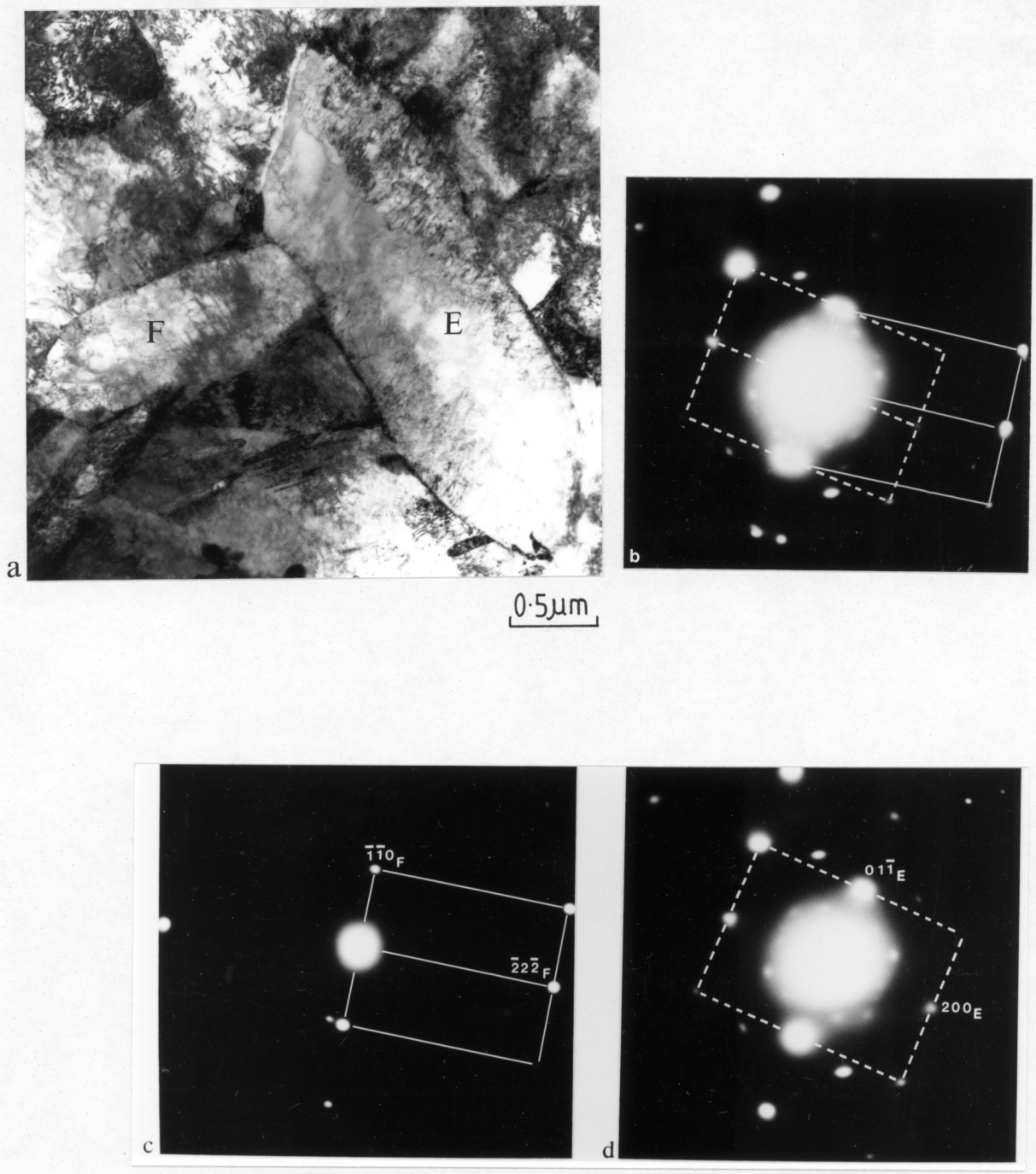

Figure VI.4 - Electron micrograph and corresponding diffraction patterns from a pair of α_a plates E and F. (a) Bright field image. (b) SADP interface of grains E and F. (c) SADP from grain F. (d) SADP from grain E. The central spots are Fe_2O_3 surface oxide reflections.

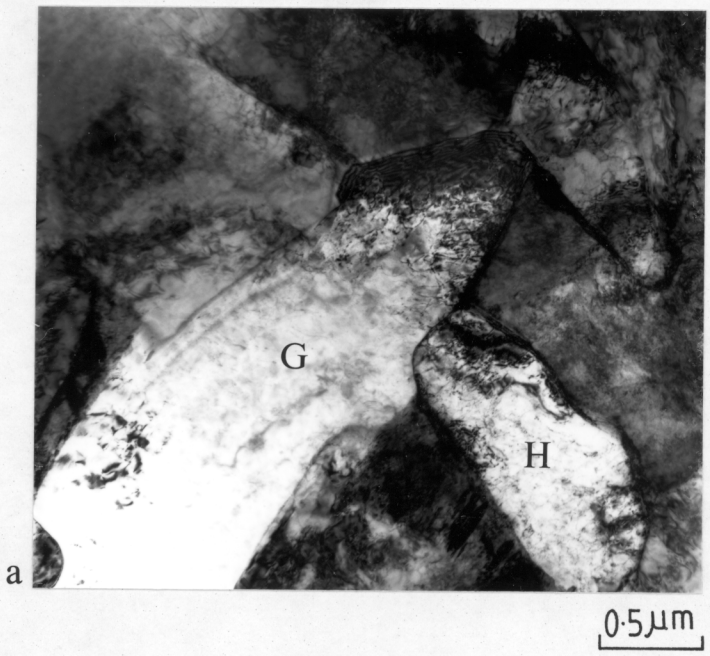

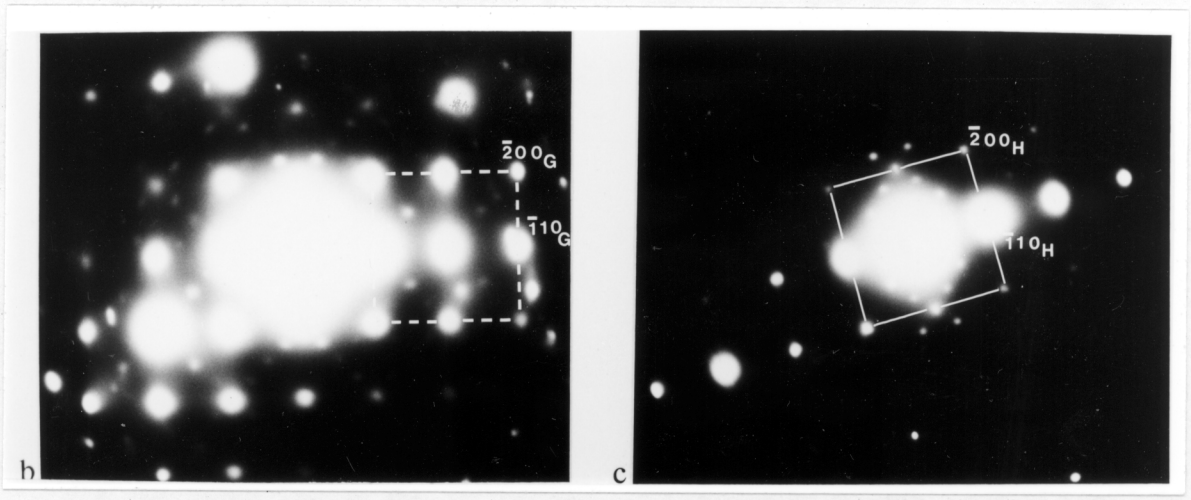

Figure VI.5 - Electron micrograph and corresponding diffraction patterns from a pair of α_a plates G and H. (a) Bright field image. (b) SADP from grain G. (c) SADP from grain H. The central bright spots are Fe_2O_3 surface oxide reflections.

Figure VI.6 - Electron micrograph shows six acicular ferrite plates designated I,J,K,L,M and N, which are in intimate contact.

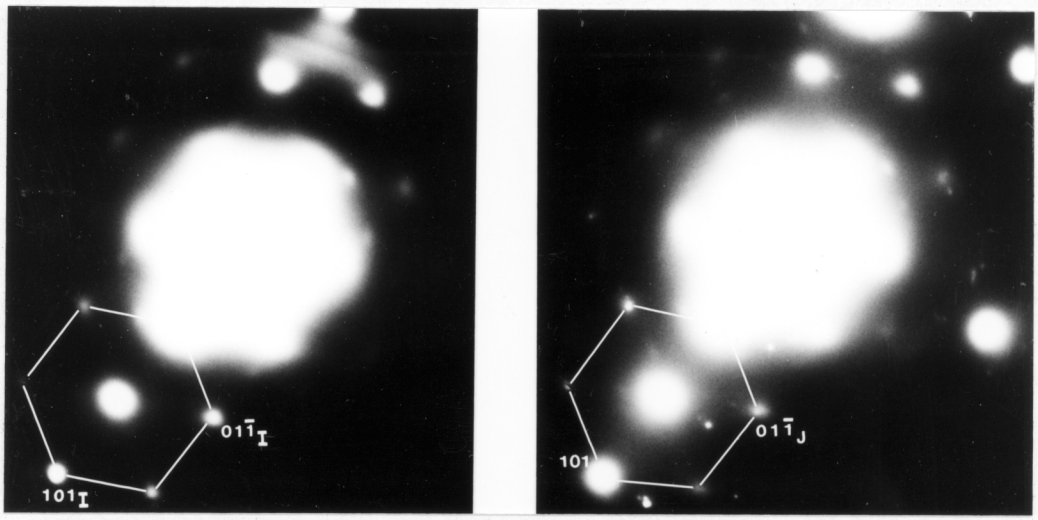

Figure VI.7 - Showing the corresponding selected area diffraction patterns (SADP) from the pair of acicular plates I and J, respectively. Details of orientation relationship are discussed in text.

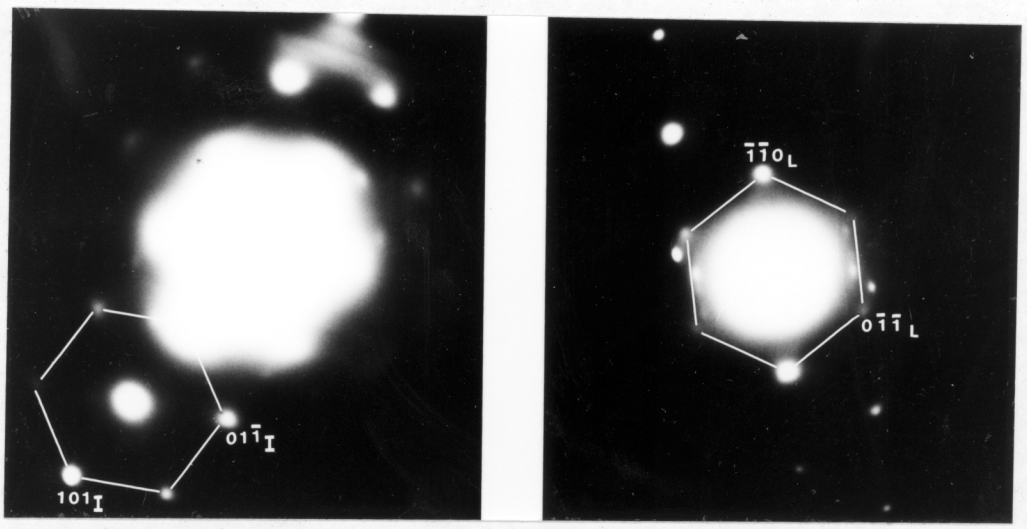

Figure VI.8 - Showing the corresponding SADP from the pair of acicular ferrite plates I and L, respectively. The axis/angle pair can be represented by <1$\bar{1}$1>/11°.

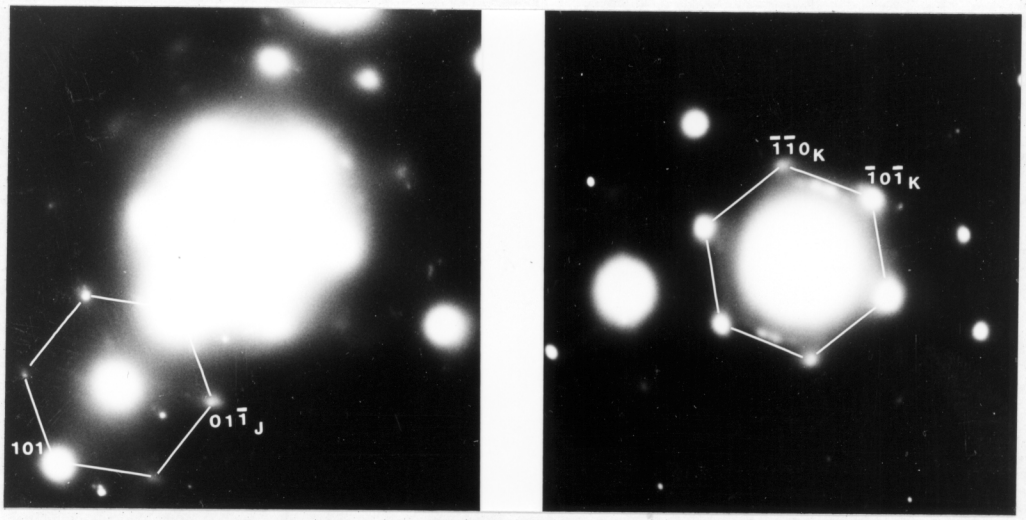

Figure VI.9 - Showing the corresponding SADP from the pair of acicular ferrite plates J and K, respectively. The axis/angle pair can be represented by <1 1 l>/11°.

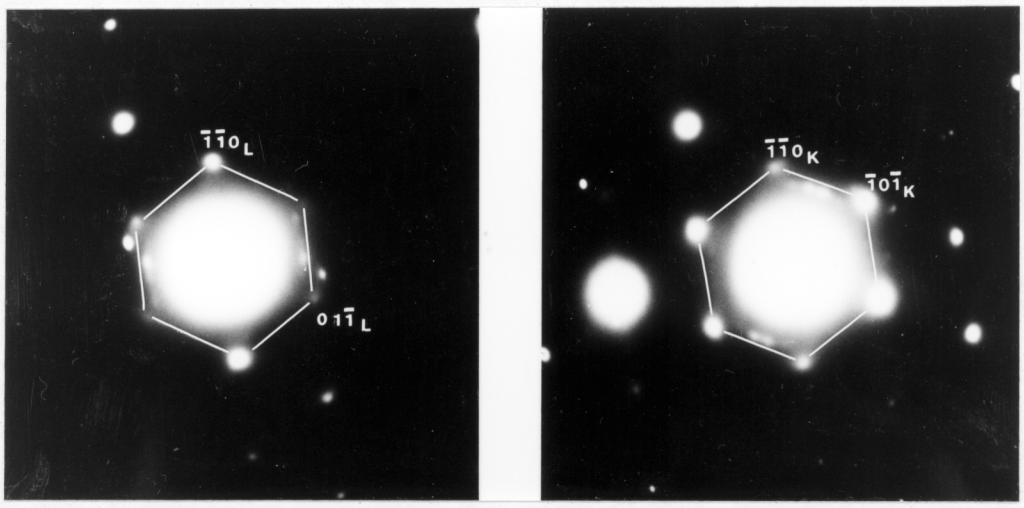

Figure VI.10 - Showing the corresponding SADP from the pair of acicular ferrite plates L and K, respectively. Details of orientation relationship are discussed in text.

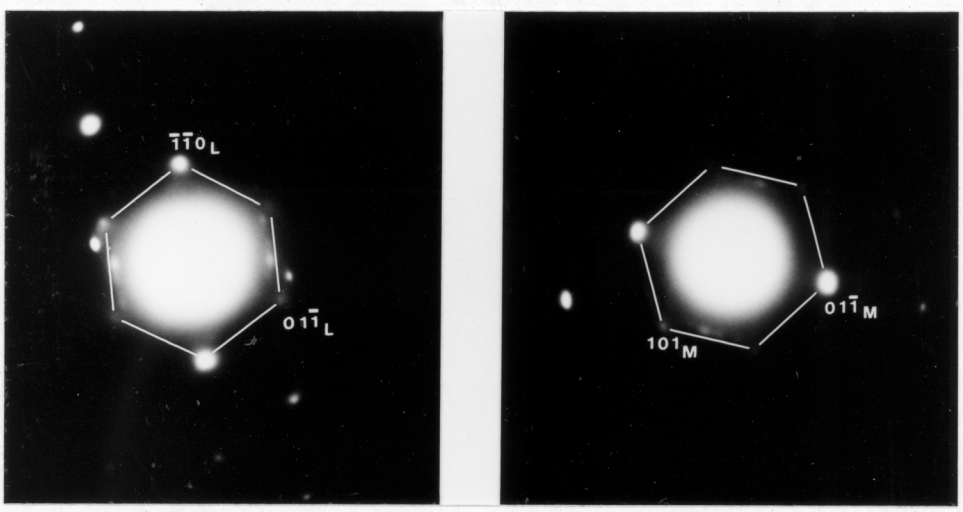

Figure VI.11 : Showing the corresponding SADP from the pair of acicular ferrite plates L and M, respectively. The axis/angle pair can be represented by <111>/8°.

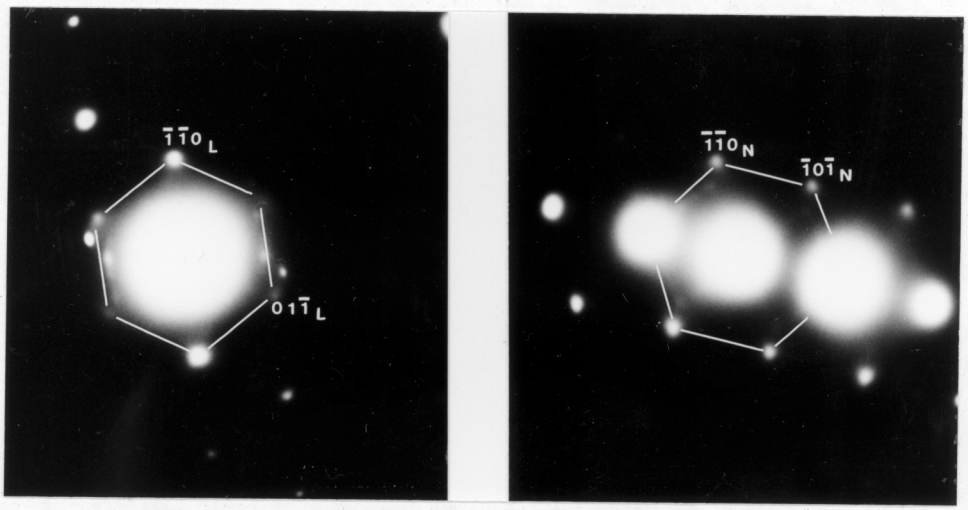

Figure VI.12 - Showing the corresponding SADP from the pair of acicular ferrite plates L and N, respectively. The axis/angle pair can be represented by <111>6°.

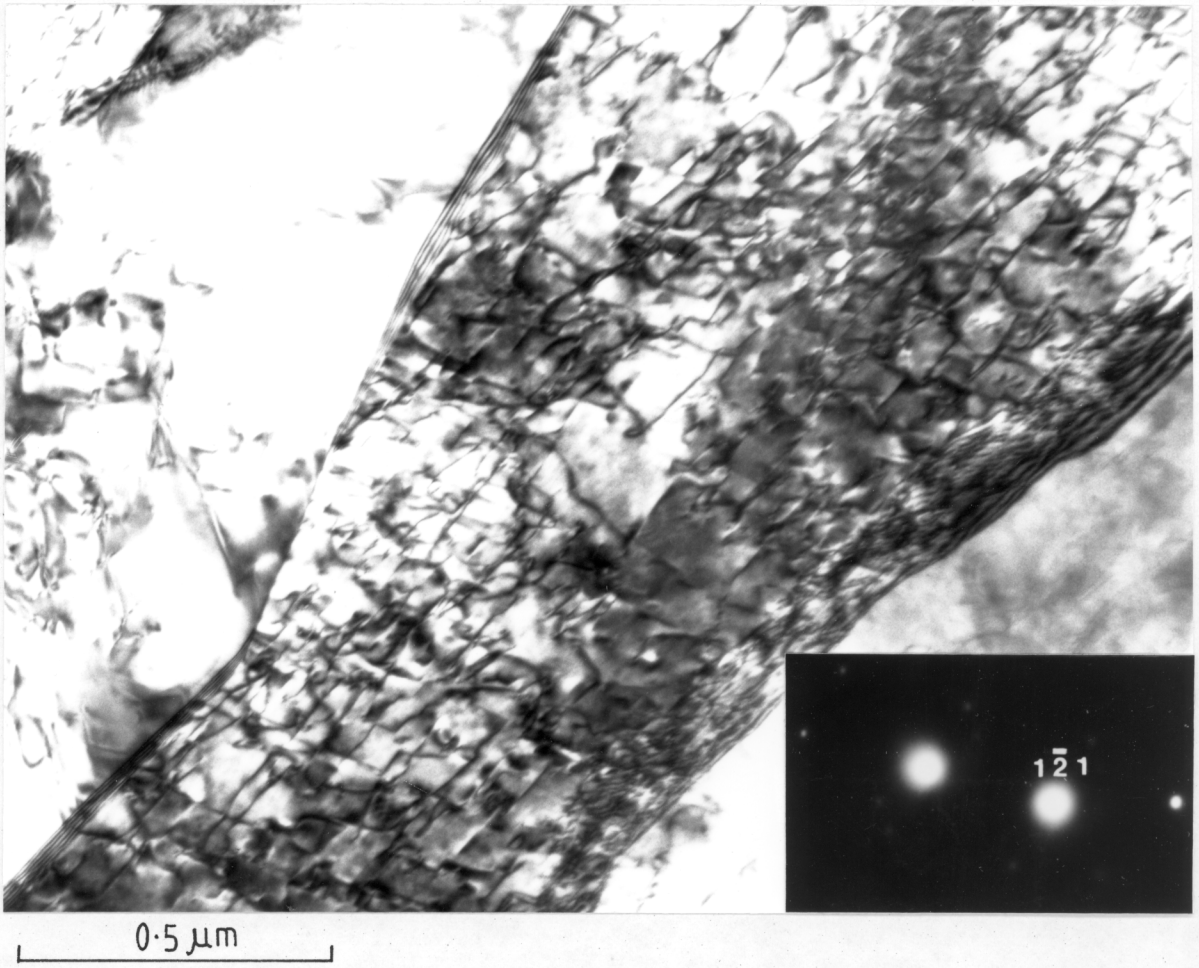

Figure VI.13 - Electron micrograph shows the bright field image of acicular ferrite under two-beam condition $\bar{g} = \langle 12\bar{1} \rangle$.